AIP | Physics of Fluids

Investigating mode competition and three-dimensional features from two-dimensional velocity fields in an open cavity flow by modal decompositions

Florimond Guéniat, Luc Pastur, and Francois Lusseyran

Citation: Physics of Fluids (1994-present) **26**, 085101 (2014); doi: 10.1063/1.4891254
View online: http://dx.doi.org/10.1063/1.4891254
View Table of Contents: http://scitation.aip.org/content/aip/journal/pof2/26/8?ver=pdfcov
Published by the AIP Publishing

Articles you may be interested in

Stability of the steady three-dimensional lid-driven flow in a cube and the supercritical flow dynamics
Phys. Fluids **26**, 024104 (2014); 10.1063/1.4864264

Three-dimensional flow features in a nominally two-dimensional rectangular cavity
Phys. Fluids **25**, 097101 (2013); 10.1063/1.4819780

A time-resolved particle image velocimetry investigation of a cavity flow with a thick incoming turbulent boundary layer
Phys. Fluids **20**, 105101 (2008); 10.1063/1.2990043

Three-dimensional numerical study of natural convection in vertical cylinders partially heated from the side
Phys. Fluids **17**, 124101 (2005); 10.1063/1.2141430

Three-dimensional instability and state selection in an oscillatory axisymmetric swirling flow
Phys. Fluids **14**, 3983 (2002); 10.1063/1.1509452

Vacuum Solutions from a Single Source
- Turbopumps
- Backing pumps
- Leak detectors
- Measurement and analysis equipment
- Chambers and components

PFEIFFER VACUUM

This article is copyrighted as indicated in the article. Reuse of AIP content is subject to the terms at: http://scitation.aip.org/termsconditions. Downloaded to IP: 82.230.43.64 On: Thu, 21 Aug 2014 14:08:28

PHYSICS OF FLUIDS **26**, 085101 (2014)

Investigating mode competition and three-dimensional features from two-dimensional velocity fields in an open cavity flow by modal decompositions

Florimond Guéniat,[1,2] Luc Pastur,[1,2] and Francois Lusseyran[2]
[1]*Paris Sud University, 91400 Orsay cedex, France*
[2]*LIMSI-CNRS, 91403 Orsay cedex, France*

(Received 11 March 2014; accepted 14 July 2014; published online 1 August 2014)

Shear-layer driven open cavity flows are known to exhibit strong self-sustained oscillations of the shear-layer. Over some range of the control parameters, a competition between two modes of oscillations of the shear layer can occur. We apply both Proper Orthogonal Decomposition and Dynamic Mode Decomposition to experimental two-dimensional two-components time and spaced velocity fields of an incompressible open cavity flow, in a regime of mode competition. We show that, although proper orthogonal decomposition successes in identifying salient features of the flow, it fails at identifying the spatial coherent structures associated with dominant frequencies of the shear-layer oscillations. On the contrary, we show that, as dynamic mode decomposition is devoted to identify spatial coherent structures associated with clearly defined frequency channels, it is well suited for investigating coherent structures in intermittent regimes. We consider the velocity divergence field, in order to identify spanwise coherent features of the flow. Finally, we show that both coherent structures in the inner-flow and in the shear-layer exhibit strong spanwise velocity gradients, and are therefore three-dimensional. © *2014 AIP Publishing LLC*. [http://dx.doi.org/10.1063/1.4891254]

I. INTRODUCTION

An efficient way for understanding the intrinsic phenomenology of a flow relies on the analysis of its constitutive coherent structures. Hence, the identification and extraction of these structures has received the careful attention of many contributions in the fluid mechanics community. Even today, such an aim remains challenging, although crucial steps have been made in the last decades.

A significant improvement in coherent structures detection was achieved with the introduction of Proper Orthogonal Decomposition (POD) techniques in the 1980s.[1–3] Proper orthogonal decomposition is aimed at identifying, in a given dataset of velocity fields, patterns that are the most correlated in space and time, with respect to kinetic energy. Some spatial modes identified by proper orthogonal decomposition are sometimes considered as empirically determined coherent structures of the flow under study. Proper orthogonal decomposition proved to be very efficient in several problems where scales are clearly separated, e.g., cylinder wakes, or shear-layer self-sustained oscillations.[4,5]

However, when several temporal frequencies are relevant, and associated with coherent structures of similar size, it is not guaranteed whether proper orthogonal decomposition is still able to discriminate between the different patterns of the flow, or rather merge them into some "optimal" pattern. Substitutes to proper orthogonal decomposition have been proposed in order to empirically extract coherent structures out of a dataset, based on either eulerian[6] or lagrangian criterions.[7,8] Recently, Schmid[9] and Rowley *et al.*[10] introduced the Dynamic Mode Decomposition (DMD) as a way for approximating eigenmodes of the Koopman operator of a flow. Dynamic modes, as an approximation of Koopman modes, reveal spatial coherent structures associated with temporal spectral components, including temporal growth rates. By construction, dynamic modes are therefore expected to be relevant with respect to the dynamics of the flow.[18] After the two founding papers by

 © 2014 AIP Publishing LLC

This article is copyrighted as indicated in the article. Reuse of AIP content is subject to the terms at: http://scitation.aip.org/termsconditions. Downloaded to IP: 82.230.43.64 On: Thu, 21 Aug 2014 14:08:28

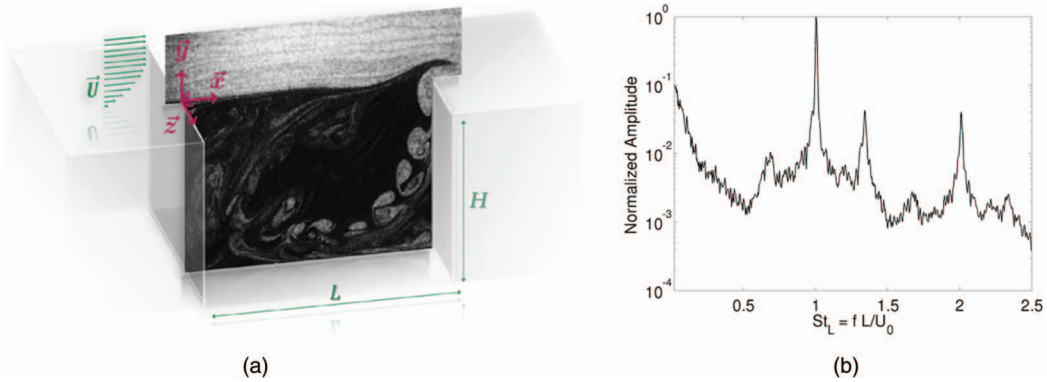

FIG. 1. (a) Smoke visualisation of the open-cavity flow, in a (x, y) plane. The Blasius' profile of the incoming laminar layer, the cavity length L and height H are represented in green. (b) Power spectrum of the flow, from Laser Doppler Velocimetry measurement at a point near the trailing edge, in the shear layer.

Rowley *et al.*[10] and Schmid,[9] many publications followed, referring to dynamic mode decomposition as a method to investigate the "dynamical squeleton" of several flows, from cavity flows[9,11] to jet flows.[12,13] Chen *et al.*[14] showed how dynamic mode decomposition and discrete Fourier transform (DFT) are connected, while Schmid[9] proposed efficient algorithms for extracting dominant frequencies and the associated dynamic modes. Although dynamic mode decomposition requires regularly sampled time-resolved fields,[15,16] showed how non-uniform DMD can overcome this constraint. Finally, Mezić[17,18] made clear the connection between dynamic mode decomposition and Koopman analysis, inherited from the dynamical system theory.

In this paper, we consider an incompressible open cavity flow subject to mode competition. Open cavity flows are long known to develop strong coherent, self-sustained oscillations into the shear layer, as it may be seen in Figure 1(a). Self-sustained oscillations are usually understood as the result of a feedback-loop mechanism. Perturbations at the cavity leading edge are amplified in the shear layer, where vorticity is produced. Vortices are advected downstream and impinge onto the cavity trailing edge. Impingement is a source of perturbation for the pressure field, which, due to incompressibility, triggers new perturbations at the leading edge, hence closing the loop.[19] On most ranges of the control parameters, only one dominant frequency characterizes the shear-layer oscillations. It can however occur, on limited ranges of the control parameters, that two dominant modes be enhanced in the shear layer (see, e.g., the pioneer work of Rockwell *et al.*,[19–21] or more recent works by Kegerise *et al.*[22] and Pastur *et al.*[23]). Consequently, the shear layer may exhibit, in time, sequences of oscillations, at either one frequency or the other. In this paper, we handle the study of such a regime from the two viewpoints of proper orthogonal decomposition and dynamic mode decomposition.

We show that proper orthogonal decomposition is actually not able to extract each coherent structure separately. Instead, the structure of the unique dominant spatial POD mode is the "barycentric mixing" of the two basic physical modes of oscillation. On the contrary, dynamic mode decomposition naturally does extract the coherent structures associated with each frequency of oscillation, separately. In the case of the cavity flow, both regimes of oscillations occur at two different frequencies. From the two dominant dynamic modes, we are able to extract wavelengths and velocities of the traveling waves in the shear layer, and recover well-known features of Kelvin-Helmholtz modes.

In addition, coherent structures are, as very often in flows, three-dimensional (3D). It can be due to boundary or forcing conditions, nonlinear saturation or secondary instabilities, etc. For instance, Kelvin-Helmholtz rolls in free shear layers hardly remain uniform in the spanwise direction but quickly experience spanwise modulations. In experimental applications, however, it is usual to deal with two-dimensional velocity fields, even though tomographic techniques are now able to give access to volumetric knowledge in the flow. Such techniques are however dedicated to restricted volumes in space and limited by the huge amount of data to be stored and processed. Therefore, finding ways to extract three-dimensional information from two-dimensional fields remains valuable

This article is copyrighted as indicated in the article. Reuse of AIP content is subject to the terms at: http://scitation.aip.org/termsconditions. Downloaded to IP: 82.230.43.64 On: Thu, 21 Aug 2014 14:08:28

approaches. Most usually, in today experiments, we have access to spatially well-resolved two-dimensional velocity fields, for instance, by using Particle Image Velocimetry techniques (PIV). Nowadays, high-speed PIV opens the door to time-resolved velocity fields and use of dynamic mode decomposition. In this paper, we take benefit of the incompressibility of the flow to determine the three-dimensional features associated with coherent structure constitutive of the flow. We are able to do so because dynamic modes can be thought of as "statistically converged representations" of salient dynamical features of the flow. Indeed, dynamic modes are coherent structures identified over an observation time that is usually much longer than the characteristic time-scale associated with the mode. In addition, we show that the spatial properties of the flow, such as incompressibility, are inherited by dynamic modes computed from the companion matrix method.[10] Moreover, because dynamic modes are "time-averaged structures," they must be smooth, where their kinetic energy is strong, if the underlying velocity field is smooth. As a consequence, it is expected that the divergence field is continuous and derivable, if non-vanishing, where the mode is energetic. Though it may seem counter-intuitive, we show that both dynamic modes, associated with shear-layer oscillations, are intrinsically three-dimensional structures of the flow. We conclude this paper by putting these results into perspective with respect to what is known from experimental and numerical studies in the literature on open cavity flows.

II. SNAPSHOT-BASED ANALYSIS

In the context of modal decomposition, the aim of snapshot-based analysis is to find a relevant basis for describing snapshots of the flow fields. Practically, snapshots are realisations of a given measure – i.e., the observable – of the dynamics.

In this section, we give a unified presentation of POD and DMD. Both decompositions are applied to the same dataset, K_0^N, made of $N+1$ snapshots ordered in time. The observable $\boldsymbol{u}(\boldsymbol{r},t)$ – for instance, realisations of the velocity field – belongs to $\mathcal{R}^{n_p}$, with $\boldsymbol{r}$ the mesh of the physical space. Realisations are sampled at every time-step δt from 0 to time $T = N\delta t$. Hence,

$$K_0^N := \{\boldsymbol{u}(\boldsymbol{r},0), \boldsymbol{u}(\boldsymbol{r},\delta t), \ldots, \boldsymbol{u}(\boldsymbol{r},(N-1)\delta t), \boldsymbol{u}(\boldsymbol{r},N\delta t)\}, \tag{1}$$

is a $n_p \times N$ matrix. Discrete time $i\delta t$ and $\boldsymbol{u}(\boldsymbol{r},i\delta t)$ will be referred to below as $t_i \equiv i\delta t$ and $\boldsymbol{u}_i \equiv \boldsymbol{u}(\boldsymbol{r},i\delta t)$, respectively.

A. Proper orthogonal decomposition algorithm

The proper orthogonal decomposition, also known as Karhunen-Loève expansion, or principal component analysis, has been described in many articles. In the following, we briefly summarize the so-called snapshot method,[2] adapted to cases where $n_p \gg N$. The reader interested in the method may refer to Holmes *et al.*[24] or Kerschen *et al.*[25]

We look for an orthonormal basis of spatial modes $\{\boldsymbol{\psi}_i\}$, called *topos*, and temporal modes $\{\alpha_i\}$, called *chronos*, such that the average least-squares truncation error,

$$r_m = \sum_{k=0}^{N} \left\| \boldsymbol{u}(\boldsymbol{r},t_k) - \sum_{i=0}^{m} \alpha_i(t_k)\boldsymbol{\psi}_i(\boldsymbol{r}) \right\|_2, \tag{2}$$

is minimized, whatever the choice of $m \leq \operatorname{rank}\left\{K_0^N\right\} \leq N$. Here, $\|.\|_2$ is the $\mathcal{L}_2$ norm.

Solving Eq. (2) leads to the eigenvalues problem

$$\int_{\mathcal{D}} R(\boldsymbol{r},\boldsymbol{r}')\boldsymbol{\psi}_i(\boldsymbol{r}')\,\mathrm{d}\boldsymbol{r}' = \lambda_i\boldsymbol{\psi}_i(\boldsymbol{r}) \quad i = 0,\ldots,N, \tag{3}$$

with the correlation, or tensor product, matrix

$$R(\boldsymbol{r},\boldsymbol{r}') := \frac{1}{T}\int_T \boldsymbol{u}(\boldsymbol{r},t)\,\boldsymbol{u}^{\dagger}(\boldsymbol{r}',t)\,\mathrm{d}t, \tag{4}$$

This article is copyrighted as indicated in the article. Reuse of AIP content is subject to the terms at: http://scitation.aip.org/termsconditions. Downloaded to IP: 82.230.43.64 On: Thu, 21 Aug 2014 14:08:28

where † is the hermitian transpose operator. Then, for a discrete system

$$R(\boldsymbol{r},\boldsymbol{r}') = \frac{1}{N+1}\sum_{l=0}^{N}\boldsymbol{u}(\boldsymbol{r},t_l)\boldsymbol{u}^\dagger\left(\boldsymbol{r}',t_l\right) = \frac{1}{N+1}K_0^N K_0^{N\dagger}. \tag{5}$$

The dimension of R is $n_p \times n_p$. The large size of this problem implies that it may be difficult to solve. Consequently, Sirovitch[2] and Holmes *et al.*[24] proposed to rewrite the *topos* as a linear combination of the snapshots

$$\boldsymbol{\psi}_i(\boldsymbol{r}) = \sum_{k=0}^{N} a_i^k \boldsymbol{u}(\boldsymbol{r},t_k) \quad i=0,\ldots,N. \tag{6}$$

Straightforward computations show that $a_i^k = \alpha_i(t_k)$. By substituting the expansion (6) in Eq. (3), and rearranging terms, we obtain

$$\sum_{k=0}^{N}\left(\sum_{l=0}^{N}\frac{1}{N+1}\left(\int_{\mathcal{D}}\boldsymbol{u}\left(\boldsymbol{r}',t_l\right)\boldsymbol{u}^\dagger\left(\boldsymbol{r}',t_k\right)\mathrm{d}\boldsymbol{r}' a_i^l\right)\boldsymbol{u}(\boldsymbol{r},t_k)\right) = \lambda_i\sum_{k=0}^{N}a_i^k\boldsymbol{u}(\boldsymbol{r},t_k). \tag{7}$$

Then the family $\left(a_i^k\right)_{(i,k)\in\{0,\ldots,N\}^2}$ is solution of Eq. (3) as soon as

$$\sum_{l=0}^{N}\frac{1}{N+1}\left(\int_{\mathcal{D}}\boldsymbol{u}\left(\boldsymbol{r}',t_l\right)\boldsymbol{u}^\dagger\left(\boldsymbol{r}',t_k\right)\mathrm{d}\boldsymbol{r}' a_i^l\right) = \lambda_i a_i^k. \tag{8}$$

This can be rewritten as the smaller eigenvalue problem

$$\tilde{R}\boldsymbol{a}_i = \lambda\boldsymbol{a}_i \quad i=0,\ldots,N, \tag{9}$$

where $\tilde{R}$ is now a $(N+1)\times(N+1)$ matrix

$$\tilde{R} := \frac{1}{N+1}K_0^{N\dagger}K_0^N, \tag{10}$$

and $\boldsymbol{a}_i = (\alpha_i(t_k))^\dagger_{k\in\{0,\ldots,N\}} = \left(a_i^k\right)^\dagger_{k\in\{0,\ldots,N\}}$ is the projection of the i*th topos* on the snapshots, i.e., the *chronos*. $\tilde{R}$ is a symmetric and semi-definite positive matrix, therefore $\boldsymbol{a}_i$ is an orthogonal set. Formula (6), then gives the *topos*.

B. Dynamic mode decomposition algorithm

In this section, we recall the dynamic mode decomposition algorithm, based on the companion matrix, in a way which strengthen the link with the dynamical system theory, and some of its main spatial and spectral properties.

1. Evolution operator

We consider that the flow is driven by a dynamical system, evolving on a manifold $\mathcal{D}$ of dimension $n_\mathcal{D}$. Let $\boldsymbol{x}$ be the state vector of the system, in $\mathcal{D}$. Let $\phi_{\Delta t}$ be the dynamical flow from $\mathcal{D}$ to $\mathcal{D}$, driving the state from $\boldsymbol{x}(t)$ at time t to the state $\boldsymbol{x}(t+\Delta t)$ at time $t+\Delta t$, where Δt is the sampling period

$$\boldsymbol{x}(t+\Delta t) = \phi_{\Delta t}(\boldsymbol{x}(t)). \tag{11}$$

Let Π be a projection from $\mathcal{D}$ onto the observable space Ω. We assume that the dimension of Ω is n_p. Then, the observable $\boldsymbol{u}$ is defined as

$$\boldsymbol{u}(t) = \Pi(\boldsymbol{x}(t)). \tag{12}$$

This article is copyrighted as indicated in the article. Reuse of AIP content is subject to the terms at: http://scitation.aip.org/termsconditions. Downloaded to IP: 82.230.43.64 On: Thu, 21 Aug 2014 14:08:28

Π may be understood as a measure on the system, extracting the output $\boldsymbol{u}$ from the state vector $\boldsymbol{x}$. We consider the operator A such as

$$A \circ \Pi = \Pi \circ \phi_{\Delta t}, \tag{13}$$

where $\circ$ is the composition operation. This operator is closely linked to the Koopman operator. Let $\mathcal{U}$ be the Koopman operator associated with the dynamical flow $\phi_{\Delta t}$. One can verify that $\mathcal{U}_\Pi = A \circ \Pi$, with $\mathcal{U}_\Pi$ the Koopman operator applied to the projection Π. Further information about the link between DMD and a Koopman analysis are developed in Ref. 18.

The operator A has an important property, when applied to an observable

$$\begin{aligned} A\left(\boldsymbol{u}\left(t_0 + n\Delta t\right)\right) &= A \circ \Pi\left(\boldsymbol{x}\left(t_0 + n\Delta t\right)\right) \\ &= \Pi \circ \phi_{\Delta t}\left(\boldsymbol{x}\left(t_0 + n\Delta t\right)\right) \\ &= \Pi\left(\boldsymbol{x}\left(t_0 + (n+1)\,\Delta t\right)\right) \\ &= \boldsymbol{u}\left(t_0 + (n+1)\,\Delta t\right). \end{aligned} \tag{14}$$

A is an evolution operator between snapshots $\boldsymbol{u}_n$ and $\boldsymbol{u}_{n+1}$. For the sake of readability, $\boldsymbol{u}\left(t_0 + n\Delta t\right)$ will be noted as $\boldsymbol{u}_n$. The main objective of Sec. II B is to expose the dynamic mode decomposition algorithm, which aims at extracting information from the operator A, i.e., information of the dynamics itself, by the mean of an experimental dataset.

2. Construction of a similar operator

DMD algorithms rely on well known properties of similar matrices, i.e., matrices that share spectral features.

As A is *a priori* not known, the only way to build a similar matrix to A is from the dataset itself. If K_i^j is the dataset of observable, orderly in increasingly time, i.e., $K_i^j = \left\{\boldsymbol{u}_i, \boldsymbol{u}_{i+1}, \ldots, \boldsymbol{u}_{j-1}, \boldsymbol{u}_j\right\}$, then

$$\begin{aligned} AK_i^j &= \left\{A\boldsymbol{u}_i, \ldots, A\boldsymbol{u}_j\right\} \\ &= \left\{\boldsymbol{u}_{i+1}, \ldots, \boldsymbol{u}_{j+1}\right\} \\ &= K_{i+1}^{j+1}. \end{aligned} \tag{15}$$

Therefore, we will assume the relation

$$AK_0^{N-1} = K_1^N. \tag{16}$$

For reasons that will become clear later, we make use of the companion matrix method.[10] The assumption is made that the $(N+1)$ th observable is linearly dependant from the first N vectors of the dataset K_0^N. This hypothesis is most usually relevant. At some point, adding more snapshots will not add any furthermore information. Nevertheless, it implies that A is approximated as a linear mapping operator. Then, $\boldsymbol{u}_N$ can be expressed as

$$\boldsymbol{u}_N = s_0\boldsymbol{u}_0 + s_1\boldsymbol{u}_1 + \ldots + s_{N-1}\boldsymbol{u}_{N-1} + \boldsymbol{\xi}, \tag{17}$$

where $\boldsymbol{\xi}$ is a residue. Unknown elements s_i are easily computed through a norm minimization

$$\boldsymbol{s}_{opt} = \min_{\boldsymbol{s}} \left\| \boldsymbol{u}_N - \sum_{j=0}^{N-1} s_j \boldsymbol{u}_j \right\|_2. \tag{18}$$

The norm minimization can be achieved, for instance, through an oblique projection of the last snapshot $\boldsymbol{u}_N$ onto the snapshot set K_0^{N-1}

$$\boldsymbol{s}_{opt} = \left(K_0^{N-1^\dagger} K_0^{N-1}\right)^{-1} K_0^{N-1^\dagger} \boldsymbol{u}_N. \tag{19}$$

This article is copyrighted as indicated in the article. Reuse of AIP content is subject to the terms at: http://scitation.aip.org/termsconditions. Downloaded to IP: 82.230.43.64 On: Thu, 21 Aug 2014 14:08:28

Then, it comes, from Eq. (16)

$$K_1^N = K_0^{N-1} S + R.$$

R is a residue matrix. S may be expanded as a companion matrix. It transforms the ith snapshot into the $(i+1)$th snapshot, except for the last one which is expanded as in Eq. (17)

$$S = \begin{pmatrix} 0 & \dots & \dots & 0 & s_0 \\ 1 & 0 & & \vdots & s_1 \\ 0 & 1 & \ddots & \vdots & s_2 \\ \vdots & \ddots & \ddots & 0 & \vdots \\ 0 & \dots & 0 & 1 & s_{N-1} \end{pmatrix}. \tag{20}$$

When R is neglected, the matrix S is similar to $\widehat{A} := K_0^{N-1} K_0^{N-1^\dagger} A$, the approximation of A in the image space of K_0^{N-1}

$$\widehat{A} K_0^{N-1} := K_0^{N-1} K_0^{N-1^\dagger} A K_0^{N-1} = K_0^{N-1} S. \tag{21}$$

When the companion matrix is built on the fluctuating flow fields, Chen *et al.*[14] showed that DMD is equivalent to DFT. In that case, the companion matrix has no more unknown coefficients. Equation (17) reduces to $\sum_{k=0}^{N} \boldsymbol{u}_k = \mathbf{0}$, hence $s_0 = s_1 = \dots = s_{N-1} = -1$.

Note that S is a sparse matrix, which may be not well-conditioned with noisy dataset. Alternative algorithms have been proposed to improve the matrix conditioning, for instance, through a singular value decomposition of the dataset matrix, introduced by Schmid,[9] or by constructing a Hessenberg matrix.[16] The difference between these methods is mainly the pre-conditioner.[16]

3. Extraction of modes of the evolution operator

Equation (21) gives access to a matrix similar to A, expressed in the image space of K_0^{N-1}. Therefore, eigenvalues λ_i of S are eigenvalues of the evolution operator, and from eigenvectors $\boldsymbol{\Phi}_i$ of S follow the eigenvectors $\boldsymbol{\Phi}_i \equiv K_1^N \boldsymbol{\Phi}_i$ of the operator.

The eigenvectors of A are called *dynamical modes*. If the eigenspace of the operator A is sufficiently large, then any observable can be approximated on the span of the modes $\{\boldsymbol{\Phi}_1, \dots, \boldsymbol{\Phi}_N\}$

$$\boldsymbol{u}_n = \sum_i a_i^n \boldsymbol{\Phi}_i + \boldsymbol{\xi}, \ \forall n \in \mathbb{N}, \tag{22}$$

where $\boldsymbol{\xi}$ is a residue vector. The a_i^ns are the projection coefficients resulting from the projection of $\boldsymbol{u}_N$ on the eigenspace of the operator.

C. Properties of DMD modes

1. Spectral properties

A is an evolution operator. Hence, if the residue $\boldsymbol{\xi}$ is neglected and applying A to Eq. (22), one gets

$$\begin{aligned} A\boldsymbol{u}_n &= \boldsymbol{u}_{n+1} \\ &= A \textstyle\sum_i a_i^n \boldsymbol{\Phi}_i \\ &= \textstyle\sum_i A a_i^n \boldsymbol{\Phi}_i \\ &= \textstyle\sum_i a_i^n \lambda_i \boldsymbol{\Phi}_i, \end{aligned}$$

since $\boldsymbol{\Phi}_i$ are eigenvectors of A for the eigenvalues λ_i. Then, by recurrence, one gets

$$\boldsymbol{u}_n = \sum_i a_i^0 \lambda_i^n \boldsymbol{\Phi}_i, \tag{23}$$

This article is copyrighted as indicated in the article. Reuse of AIP content is subject to the terms at: http://scitation.aip.org/termsconditions. Downloaded to IP: 82.230.43.64 On: Thu, 21 Aug 2014 14:08:28

for any $n \in \mathbb{N}$. As each λ is complex, it may be rewritten as

$$\lambda = \rho \exp\left(\sqrt{-1}\omega \Delta t\right). \tag{24}$$

Any eigenvalue is related to a frequency channel $f = \omega/2\pi$. The dynamics of individual mode is, therefore, an harmonic oscillation at a single frequency. Equation (24) also implies that transient states can be caught by the DMD decomposition. When an eigenvalue has a modulus ρ different from unity, the mode is in a transient state. In case of a modulus larger than unity, the associated mode amplitude grows over time. Conversely, a modulus less than unity denotes a decaying behavior in time. In the following, it is assumed that $|\rho_i| = 1$.

Consequently, a spectrum may be built, by associating the mode amplitude to the corresponding frequency channel.

2. Spatial properties inheritance

Another property of DMD modes, as defined in Sec. II B 3, lies in their inheritance of spatial features of the observable, as soon as the dynamics evolve on an attractor. In such a case, growth rates are unitary.[10] Let us take the divergence field as an example. Similar calculus may be done for any linear spatial operator. When the flow regime is incompressible, then the velocity field is divergence free

$$\nabla \cdot \boldsymbol{u}(\boldsymbol{r}, t) = 0. \tag{25}$$

By using Eq. (23) for the velocity

$$\begin{aligned} \nabla \cdot \boldsymbol{u}(\boldsymbol{r}, t) &= \nabla \cdot \left(\textstyle\sum_i \mathrm{e}^{\sqrt{-1}\omega_i t} \boldsymbol{\Phi}_i(\boldsymbol{r})\right) \\ &= \textstyle\sum_i \nabla \cdot \left(\mathrm{e}^{\sqrt{-1}\omega_i t} \boldsymbol{\Phi}_i(\boldsymbol{r})\right) \\ &= \textstyle\sum_i \mathrm{e}^{\sqrt{-1}\omega_i t} \nabla \cdot \boldsymbol{\Phi}_i(\boldsymbol{r}) \\ &= 0. \end{aligned} \tag{26}$$

Then, by multiplying both side by $\mathrm{e}^{-\sqrt{-1}\omega_j t}$, we have

$$\mathrm{e}^{-\sqrt{-1}\omega_j t} \times \sum_i \mathrm{e}^{\sqrt{-1}\omega_i t} \nabla \cdot \phi_i(\boldsymbol{r}) = \sum_i \mathrm{e}^{\sqrt{-1}\omega_j t} \times \mathrm{e}^{\sqrt{-1}\omega_i t} \nabla \cdot \boldsymbol{\Phi}_i(\boldsymbol{r}),$$

which is still equal to zero. Then, if we integrate over time, as the $\mathrm{e}^{-\sqrt{-1}\omega_j t}$ form an orthonormal basis for the functional space, $\int_{-\infty}^{\infty} \mathrm{e}^{-\sqrt{-1}\omega_j t} \times \mathrm{e}^{\sqrt{-1}\omega_i t} \mathrm{d}t = \delta(i, j)$ and

$$\begin{aligned} \int_{-\infty}^{\infty} \textstyle\sum_i \mathrm{e}^{-\sqrt{-1}\omega_j t} \mathrm{e}^{\sqrt{-1}\omega_i t} \nabla \cdot \Phi_i(\boldsymbol{r}) \, \mathrm{d}t &= \textstyle\sum_i \nabla \cdot \boldsymbol{\Phi}_i(\boldsymbol{r}) \int_{-\infty}^{\infty} \mathrm{e}^{-\sqrt{-1}\omega_j t} \mathrm{e}^{\sqrt{-1}\omega_i t} \mathrm{d}t \\ &= \nabla \cdot \boldsymbol{\Phi}_j(\boldsymbol{r}) \\ &= 0. \end{aligned} \tag{27}$$

Henceforward, as for the observable $\boldsymbol{u}$, the divergence of each dynamic mode is zero. As above-mentioned, this property relies on the fact that growth rates are unitary. However, for numerical issues, we take benefit of the companion matrix algorithm, which forces growth rate values to one, as soon as the decomposition is computed from fluctuation fields.

The reader may note that, for POD, as the *chronos* also form an orthonormal basis, the *topos* also inherit spatial properties of the flow, as pointed out by Rempfer and Fasel.[26]

Even though tomographic techniques now give access to full three-dimensional velocity fields, it is still uncommon to access to three-dimensional three-components time-resolved velocity fields. Consequently, capturing three-dimensional features from two-dimensional two-components (2D2C) velocity fields remains useful. In the forthcoming part of the paper, we compare the coherent structures identified by proper orthogonal decomposition and dynamic mode decomposition in an experimental open cavity flow subject to mode competition. The velocity fields are produced by time-resolved particle image velocimetry. From the 2D2C extracted coherent structures, we will be able to infer the out-of-plane flow dynamics.

This article is copyrighted as indicated in the article. Reuse of AIP content is subject to the terms at: http://scitation.aip.org/termsconditions. Downloaded to IP: 82.230.43.64 On: Thu, 21 Aug 2014 14:08:28

III. EXPLORATION OF MODE INTERMITTENCY AND 3D FEATURES OF AN EXPERIMENTAL OPEN CAVITY FLOW

Open cavity flows are known to develop strong self-sustained oscillations. Most of the time, a single dominant mode of oscillation characterizes the flow regime, but close to transitions from one mode of oscillation to the other, there exists a small range of the Reynolds number over which two modes may coexist in the spectrum.[27] The shear layer may then oscillate at one of these frequencies or the other, alternatively in time. As a result, the flow regime is characterized by a mode-switching phenomenon, with succession of oscillations at one frequency or the other. Of course, both modes of oscillations are topologically strongly correlated, since they both involve traveling waves, at different wavelengths in the shear layer. In this case, it is expected that proper orthogonal decomposition be unable to discriminate the two modes of oscillation into two distinguishable POD modes, while dynamic mode decompositionshould, since it is based on the spectral features of the phenomenon.

A. Experimental setup

The cavity scheme is shown in Figure 1(a). The aspect ratio, cavity length L over height H, is $L/H = 2$, with $L = 100$ mm. The incoming velocity at the leading wall ($x = 0$) is $U_0 = 1.90$ m/s, corresponding to a Reynolds number around $\mathrm{Re}_L = U_0 L/\nu_{\mathrm{air}} = 12\,700$. Time-resolved particle image velocimetry allows to get time and space resolved velocity fields. The sampling frequency is 250 Hz for the velocity fields, to be compared to the dominant frequency in the flow, of the order of 30 Hz. The dataset is made of $N = 4096$ velocity fields. Much information about the setup can be found in Ref. 28.

A power spectrum of the flow, obtained by Laser Doppler Velocimetry (LDV), is shown in Figure 1(b). The time series come from a point near the impinging edge, in the shear layer. It exhibits two main peaks, at Strouhal numbers $St_L = fL/U_0 = 1.02$ and $St_L = 1.38$, where f is the frequency. In the spectrogram of Figure 2, it is observed that both modes usually do not exist continuously in time but rather rise intermittently. The spectrogram is computed by using a sliding Fourier analysis on a LDV time series. Most of the time, only one mode of shear-layer oscillation is observed at a time, which indicates that both spectral modes are in competition.

B. POD analysis

The spectrum of POD singular values is shown in Figure 3. The proper orthogonal decomposition identifies five main modes, which collect 42% of the total energy. The spatial structure of the associated *topos* are shown in Figure 4. Both the velocity field (arrows) and the vorticity field (colormap) are represented. The first mode (Figure 4(a)) is very similar to the mean flow. As

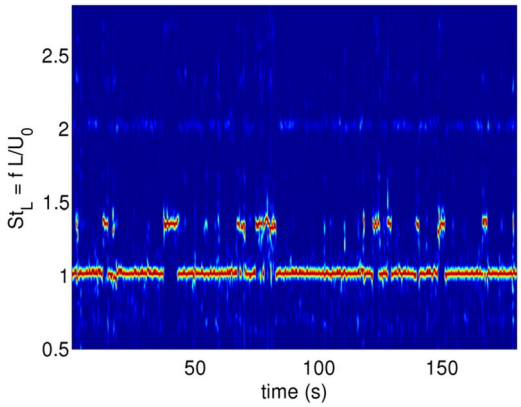

FIG. 2. Spectrogram of the flow, from a sliding Fourier analysis (step: 0.04 s, width: 2 s) from the LDV time series. Mode competition is highlighted.

This article is copyrighted as indicated in the article. Reuse of AIP content is subject to the terms at: http://scitation.aip.org/termsconditions. Downloaded to IP: 82.230.43.64 On: Thu, 21 Aug 2014 14:08:28

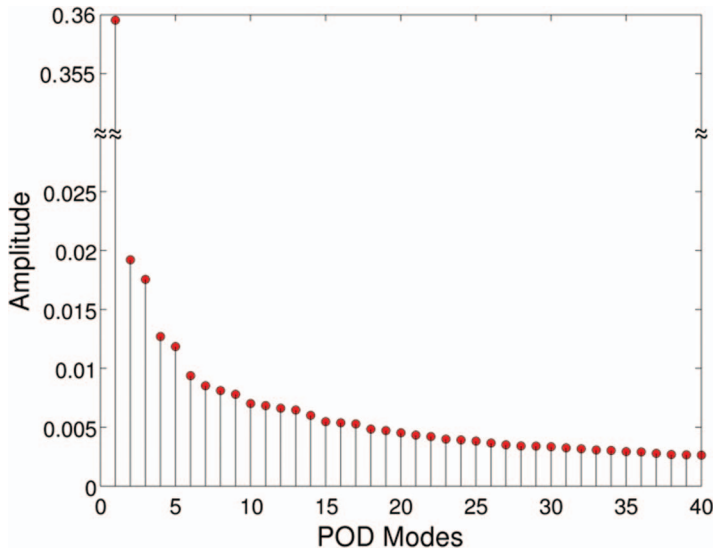

FIG. 3. Spectrum of the POD singular values for the open cavity flow experimental data-set. Amplitude is normalized by the sum of the singular values.

expected, the second and third modes (Figures 4(d) and 4(g)) exhibit coherent traveling waves in the shear layer. In addition, they are associated with singular values of the same order. Both modes look very similar, shifted one with respect to the other by a phase shift of about $\pi/2$. This is typical of conjugated modes, whose coupled dynamics reproduce traveling waves from the upstream to the downstream corner.

The fourth (Figure 4(j)) and fifth (Figure 4(m)) modes are inner flow modes, corresponding to very low frequencies, as shown in the spectrum of Figures 4(k) and 4(n).

A spectrum analysis of the second and third *chronos* reveals the two main frequencies of the flow (see Figures 4(f) and 4(i)). POD therefore behaves as a filter, rejecting from *chronos* 2 and 3 the low frequency part of the velocity power spectrum. This is coherent with the rejection, from *topos* 2 and 3, of any spatial structures but the shear-layer vortices. It is worthwhile noticing that *chronos* 2 and 3 exhibit the temporal intermittency observed in the velocity field. This is exemplified in Figure 5 for *chronos* 2, where the *chronos* oscillations switch from one frequency to the other, at least twice within the observation time. The actual intermittency of the flow is recovered, as shown by the agreement between the spectrogram computed from the *chronos* of Figure 5(a) and the spectrogram computed on the velocity field of Figure 5(b). Spectrograms were done using a sliding window of width 2 s. *Chronos* 3 produces a spectrogram similar to the spectrogram of *chronos* 2. The spectra of *chronos* 4 and 5 clearly show that the spatial features isolated in POD modes 4 and 5 are associated with structures in the inner-flow.

The POD analysis gives only one traveling wave, where the spectrogram of Figure 2 shows that they should be two in the shear layer.

The main characteristics of the amplified traveling waves in the shear layer of *topos* 4(d) can be determined by fitting the experimental velocity profile $\boldsymbol{v}(x, y_0)$, at some given $y = y_0$, by the guess profile

$$\boldsymbol{v}_{th}(x) = \boldsymbol{v}_0 + \boldsymbol{v}_1 \exp(\sigma x) \cos\left(\frac{2\pi}{\lambda} x + \Phi\right), \tag{28}$$

where λ is the wavelength, σ the spatial growth rate, Φ a reference phase, and the $\boldsymbol{v}_i$'s normalization factors. Identification is more robust in the $\boldsymbol{e}_y$ direction, and exemplified in Figure 6 for different y_0 values. The identified wavelength is $\lambda/L = 0.43$ for the second and the third *topos*. As we will later see in Sec. III C, this wavelength — and so the associated *topos* — is not physical. Indeed, this wavelength is nothing but the weighted average of the wavelengths found for each individual mode

This article is copyrighted as indicated in the article. Reuse of AIP content is subject to the terms at: http://scitation.aip.org/termsconditions. Downloaded to IP: 82.230.43.64 On: Thu, 21 Aug 2014 14:08:28

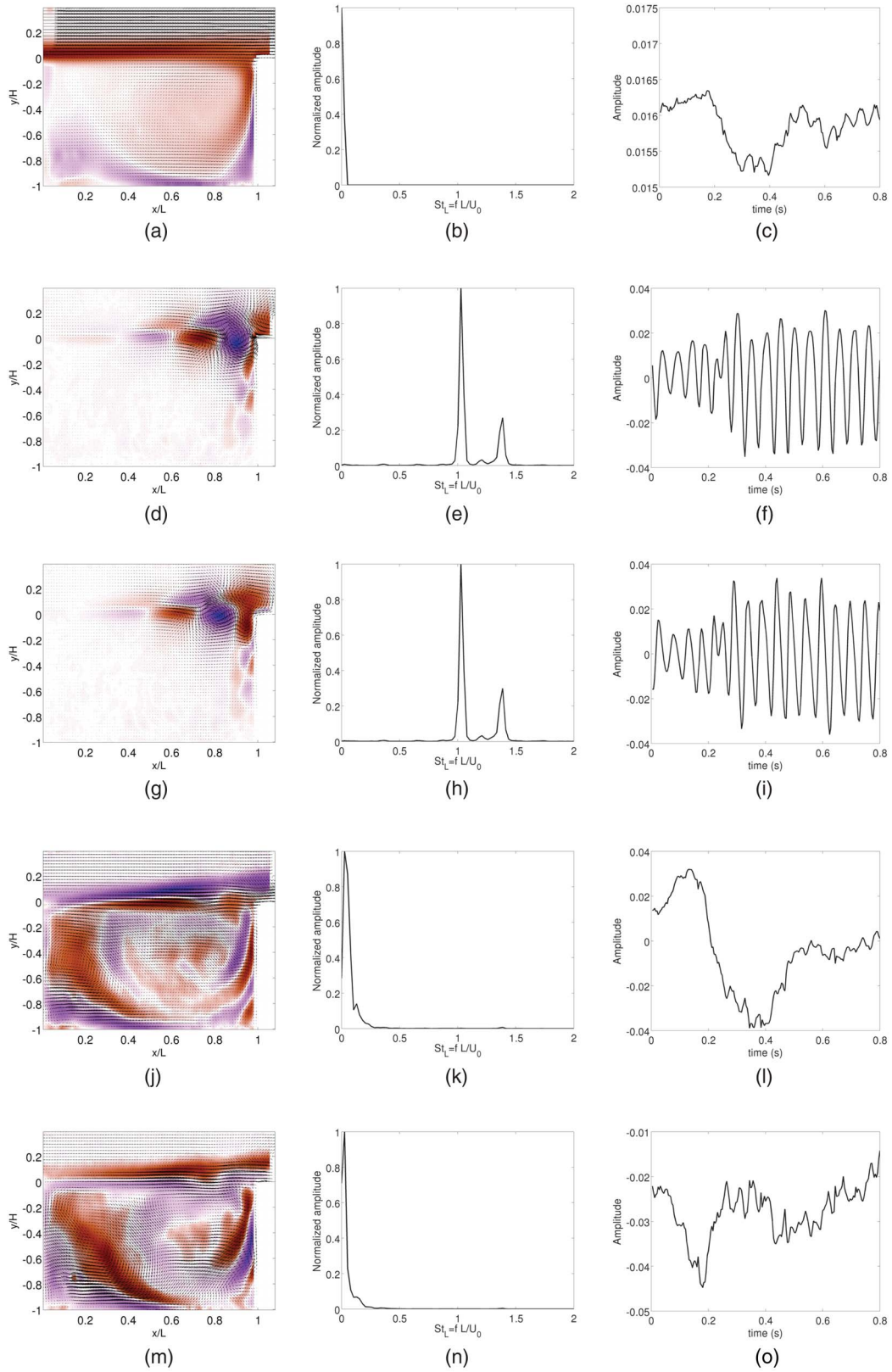

FIG. 4. From top to bottom: POD modes from 1 to 5. The color background is the vorticity field. (a), (d), (g), (j), and (m) POD *topos*. (b), (e), (h), (k), and (n) Fourier analysis of the *chronos*. (c), (f), (i), (l), and (o) sample of the *chronos.*

This article is copyrighted as indicated in the article. Reuse of AIP content is subject to the terms at: http://scitation.aip.org/termsconditions. Downloaded to IP: 82.230.43.64 On: Thu, 21 Aug 2014 14:08:28

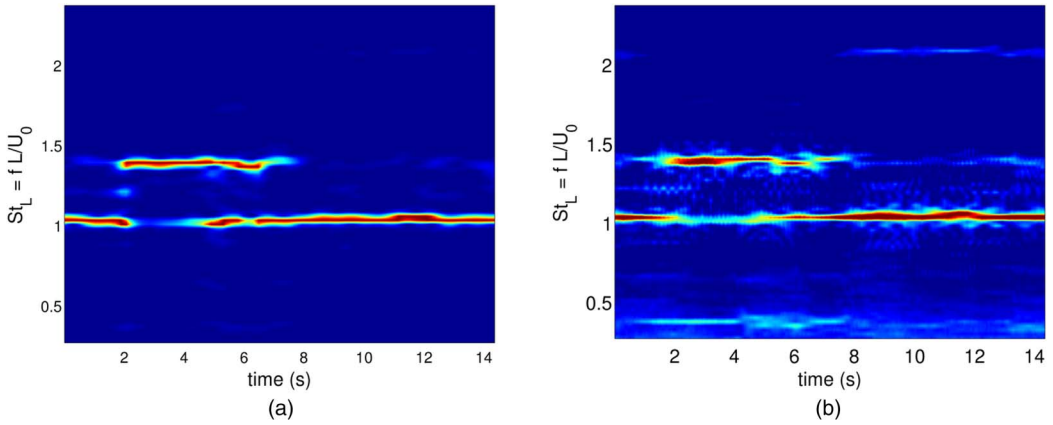

FIG. 5. Spectrograms of the flow. (a) spectrogram of *chronos* 2. (b) Mean of spectrograms, computed for each velocity component. Spectrograms are done by using a sliding FFT (step: 0.04 s, width: 2 s).

of shear-layer oscillations, in the intermittent regime. This is not surprising, since proper orthogonal decomposition detects correlated events in snapshots of the data set. Shear-layer oscillations, at whatever frequencies and wavelengths they occur, are always strongly spatially correlated to each other.

It addresses the question of the true wavelength of the shear-layer dominant mode. POD is an exact decomposition, i.e., the reconstruction of the observable, when using all the modes, is achieved with no residue. Therefore, the wavelength of the shear-layer dominant mode has to be adjusted in some way from the structure of *topos* 2–3. Some insight can be gained by considering POD modes 8–12 in Figures 7(a)–7(m). *Topos* 8–12 exhibit characteristic shear-layer vortices, coupled to inner-flow structures. This is confirmed by the power spectra of the associated *chronos*, which all exhibit the dominant frequencies of the shear-layer, together with a broad peak at very low frequency. Such modes are therefore expected to be involved in adjusting the wavelength of the train of vortices, in the shear layer. Indeed, the weighted sum of modes may describe the modification over time of the shape of a coherent structure.[26] To verify if such a superposition is responsible for the change in wavelength, one can approximate the observable $\boldsymbol{u}$ with the few involved POD spatial modes. Hence, we construct the observable $\boldsymbol{u}_{ROM}$ based on *topos* 2–12

$$\boldsymbol{u}_{ROM}(\boldsymbol{r}, t_i) = \sum_{k=2}^{12} \alpha_k(t_i)\, \boldsymbol{\Phi}_k(\boldsymbol{r}). \tag{29}$$

The first mode is not used in order to be able to fit $\boldsymbol{u}_{ROM}$ with Eq. (28).

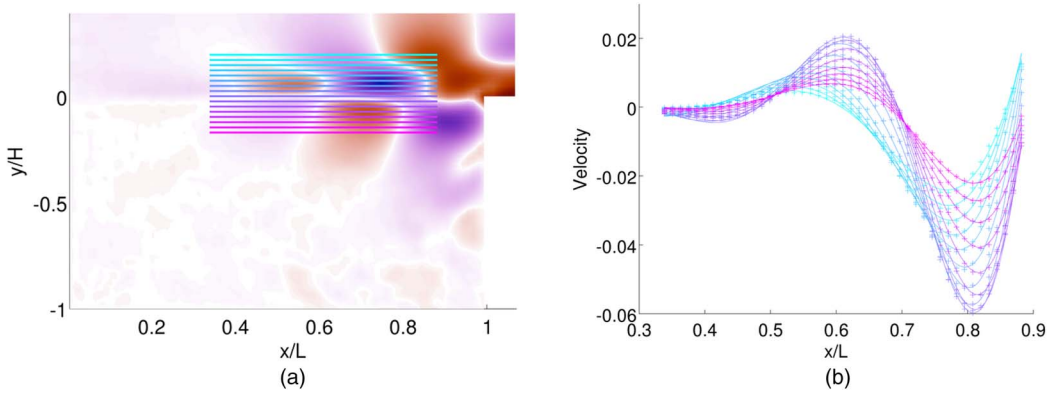

FIG. 6. Extraction of the shear layer structure wavelength. (a) Velocity y-component of the second POD *topos*. (b) Data (crosses) and fit (solid line) according to Eq. (28). Colors in (b) correspond to colored lines in figure (a).

This article is copyrighted as indicated in the article. Reuse of AIP content is subject to the terms at: http://scitation.aip.org/termsconditions. Downloaded to IP: 82.230.43.64 On: Thu, 21 Aug 2014 14:08:28

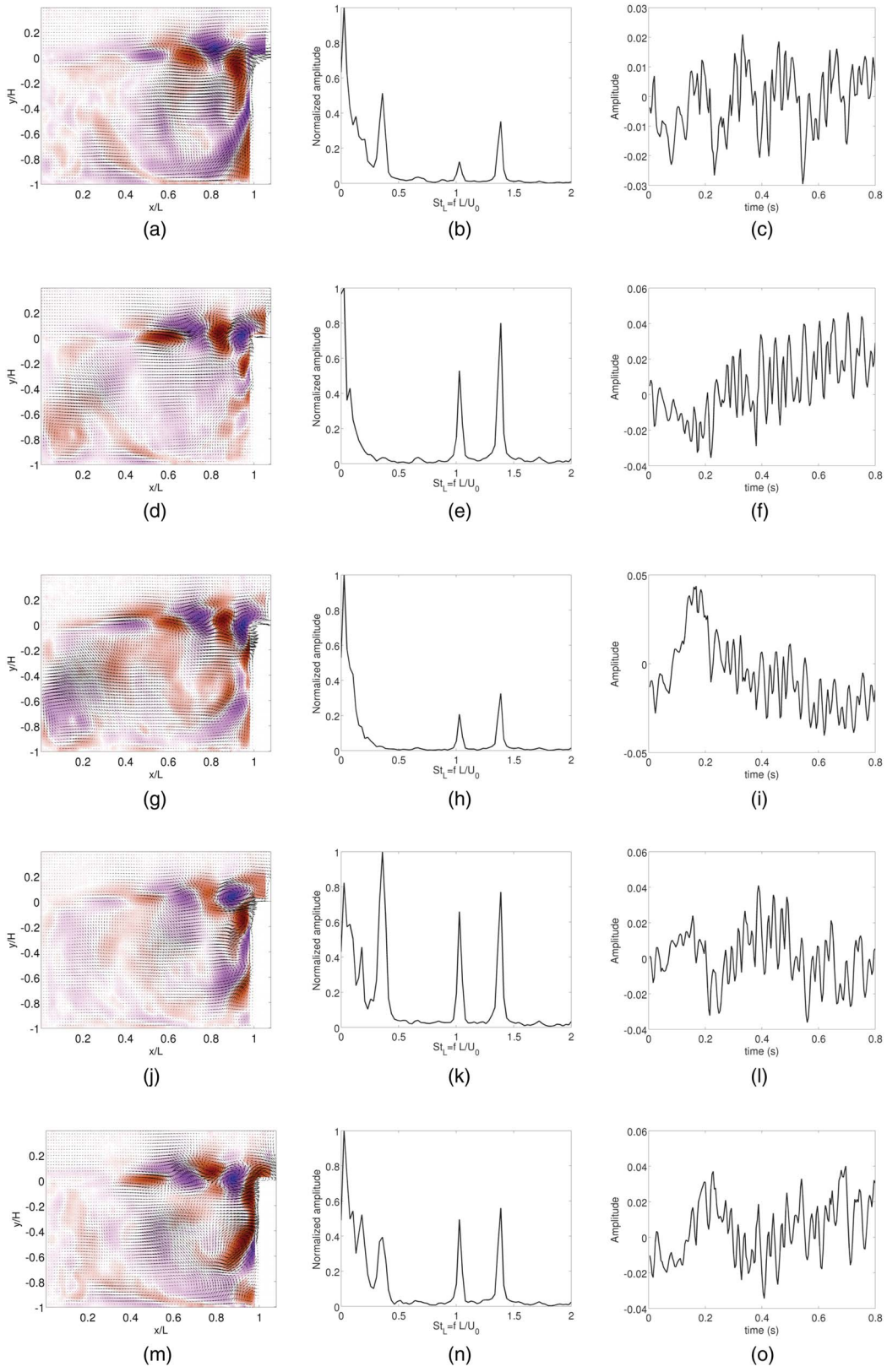

FIG. 7. From top to bottom: POD modes from 8 to 12. The color background is the vorticity field. (a), (d), (g), (j), and (m) POD *topos*. (b), (e), (h), (k), and (n) Fourier analysis of the *chronos*. (c), (f), (i), (l), and (o) Sample of the *chronos*.

This article is copyrighted as indicated in the article. Reuse of AIP content is subject to the terms at: http://scitation.aip.org/termsconditions. Downloaded to IP: 82.230.43.64 On: Thu, 21 Aug 2014 14:08:28

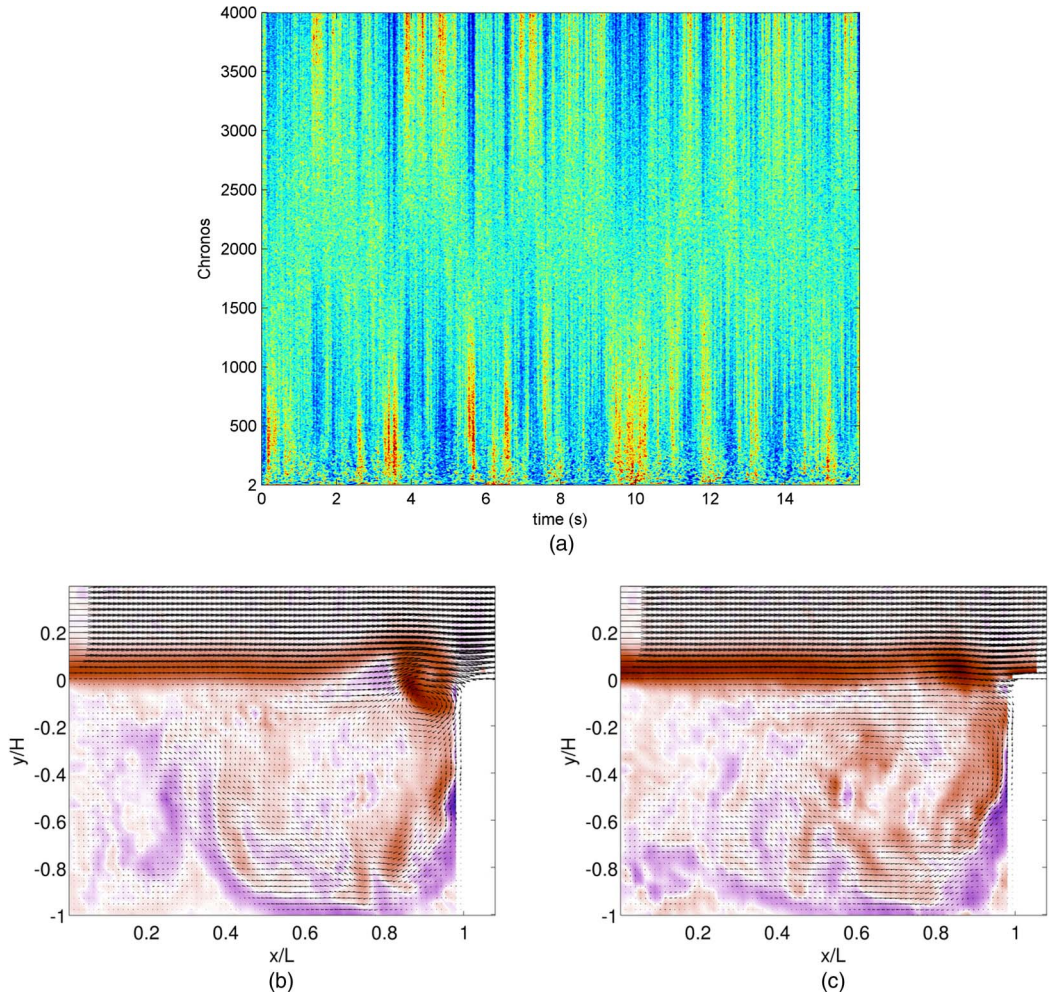

FIG. 8. (a) Amplitude of all *chronos* over time. Blue (darker grey) is for low intensity of the *chronos*, and red (light grey) is for high intensity. (b) and (c) Velocity fields associated with strong (at $t = 9.26$ s) and weak (at $t = 4.93$ s) *chronos* amplitudes for the first 200 *chronos*. The color background is the vorticity field.

The wavelength is correlated to the frequency which actually dominates in the flow. For instance, for $t_1 = 0.5$ s, the dominant frequency in the shear layer corresponds to a Strouhal number 1.02. The computed wavelength from $\boldsymbol{u}_{ROM}(t_1)$ is $\lambda/L = 0.50$. At $t_2 = 4$ s, the oscillations occur at the second frequency (Strouhal number 1.38). Then, the computed wavelength of oscillations in the shear layer, from $\boldsymbol{u}_{ROM}(t_2)$, is $\lambda/L = 0.39$. *Topos* of secondary modes (i.e., *topos* from 8 to 12, Figures 7(a) to 7(m)) therefore allow the adaptation of the main POD modes to the actual wavelength of the flow.

POD modes 8–12 are also expected to be involved in extreme events episodically occurring in the shear-layer. The amplitudes of *chronos* from 2 to 4096 are plotted in Figure 8(a). It can be noticed that there are ranges of time where the first 2000 *chronos* are either simultaneously weak or strong. It actually coincides to particularly strong (respectively, weak) event of fluid ejection, see Figure 8(b) (respectively, 8(c)). The impinging vortex, in Figure 8(b), is well-defined and have a larger amplitude than the one from Figure 8(c). The vortex from Figure 8(b) corresponds to a strong event around time $t \approx 10$ s, whereas the weak event is also detected by the *chronos* around time $t \approx 5$ s. However, when comparing the spectrogram and the amplitude of *chronos* (see Figure 9), times of occurrence of theses events appeared to be unrelated to the switches between modes of oscillation.

It is to be noted that the amplitudes of the complementary *chronos*, namely, those beyond 2500, are opposite to the amplitude of the first 2000 *chronos*. During strong or weak events, the noise over signal ratio, respectively, decreases or increases. This is an indication that numerous POD modes

This article is copyrighted as indicated in the article. Reuse of AIP content is subject to the terms at: http://scitation.aip.org/termsconditions. Downloaded to IP: 82.230.43.64 On: Thu, 21 Aug 2014 14:08:28

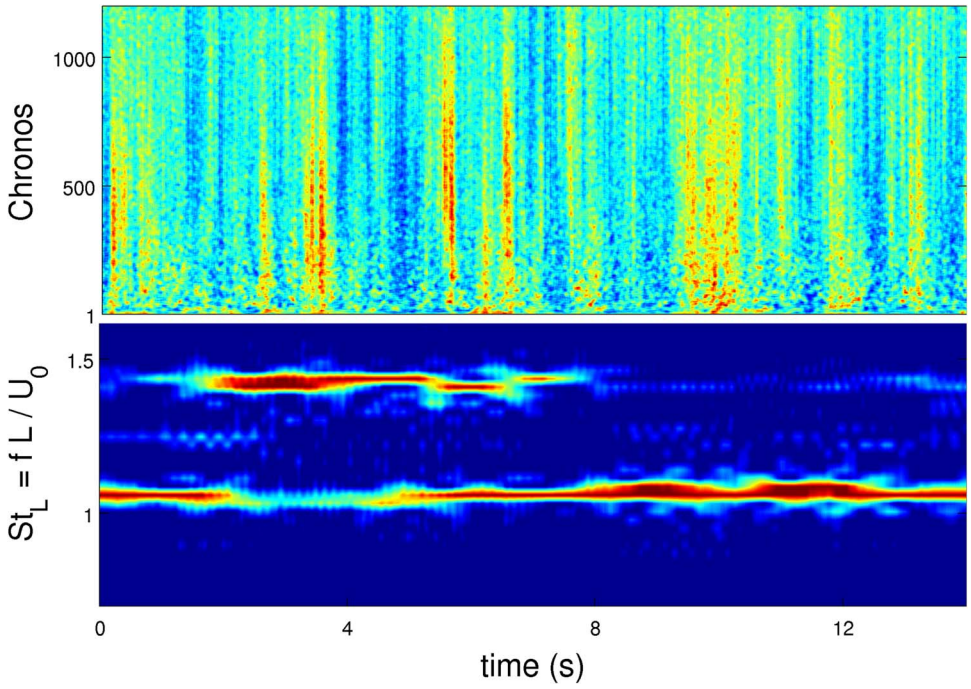

FIG. 9. Comparison between the spectrogram and the amplitude of *chronos*.

are needed for separating dynamics from noise. Henceforth, a direct POD analysis is not well-fitted for the exploration of intermittent regimes in the cavity flow because many modes are required for recovering the mode-switching phenomenon.

Instead, we could use either conditional POD for identifying each individual mode of shear-layer oscillations or dynamical mode decomposition, which is the subject of Sec. III C.

C. DMD analysis

Dynamic mode decomposition is performed on the whole dataset. The dynamics is driven by two high frequencies and some main low frequencies, as can be seen in the DMD spectrum of Figure 10. The two leading frequencies correspond to Strouhal numbers $\mathrm{St}_1 = 1.02$ and $\mathrm{St}_2 = 1.38$, which are precisely the frequencies of the shear-layer oscillations, as measured by other means. The spatial structure of the dynamical modes associated with those two Strouhal numbers are presented in Figure 11. As expected, they are energetic in the shear layer and exhibit amplified traveling waves (for instance, compare real and imaginary parts for the first dynamic mode, in Figures 11(a) and 11(b), which are shifted by a phase of about $\pi/2$). We can apply the same procedure as in Sec. III B for extracting the wavelength associated with each dynamic mode. It is found $\lambda_1/L = 0.49$ and $\lambda_2/L = 0.38$ (see Table I) for the wavelength associated with St_1 and St_2, respectively.

The velocity of the shear-layer traveling waves are therefore $c_1/U_0 = 0.50$ and $c_2/U_0 = 0.52$, respectively, typical of Kelvin-Helmholtz instabilities in free shear-layers.

It is worthwhile noticing that the wavelength found for the dominant POD mode was $\lambda_{POD}/L = 0.43$. Yet, $(\gamma_1\lambda_1/L + \gamma_2\lambda_2/L)/(\gamma_1 + \gamma_2) = 0.44 \simeq \lambda_{POD}/L$, where $\gamma_1 = 1$ and $\gamma_2 = 0.67$ are the relative amplitudes of frequencies f_1 and f_2 in the power spectrum (red or gray curve in Figure 12(d)). Therefore, λ_{POD} appears to be the weighted averaged value of λ_1 and λ_2, as shown in Figure 12.

The dynamic modes associated with Strouhal numbers $\mathrm{St} = 0.097$ and $\mathrm{St} = 0.33$ are shown in Figure 13. They exhibit patterns in the inner-flow.

Real and imaginary parts of the dynamic mode at $St = 0.097$ are close to a phase opposition, meaning that the mode is exhibiting features ascribable to a standing wave. The mode at $St = 0.33$

This article is copyrighted as indicated in the article. Reuse of AIP content is subject to the terms at: http://scitation.aip.org/termsconditions. Downloaded to IP: 82.230.43.64 On: Thu, 21 Aug 2014 14:08:28

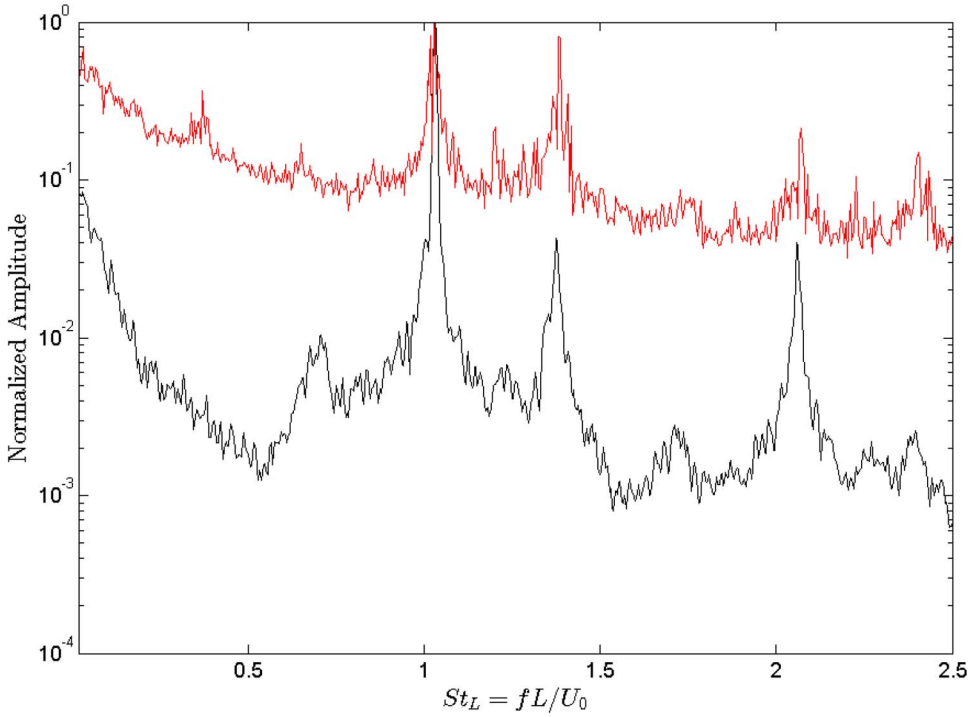

FIG. 10. Power spectrum of the flow, from Laser Doppler Velocimetry measurement at a point near the trailing edge, in the shear layer (black). The DMD spectrum (red) is computed by associating the $\mathcal{L}r$ norm of each mode to its corresponding frequency.

results from nonlinear interactions between both main shear layer modes, through triadic resonance. It is worth noticing that the resulting mode is energetic along the cavity trailing edge, where vorticity is cyclically injected inside the cavity.

Strouhal numbers were computed based on the cavity length L. When based on the cavity height H, $St_L = 0.028$ corresponds to $St_H = 0.014$, at which value structures resulting from centrifugal instabilities are known to develop inside the cavity (see Faure *et al.*[30,31] and Basley[29]). As expected, the dynamic mode in Figures 13(e) and 13(f) reveal large structures associated with the inner-flow.

D. Three-dimensional flow organisation

The present study is based on two-dimensional two-component velocity fields. However, variations of the out-of-plane component can be revealed in the divergence flow field. The flow under study is incompressible. As a consequence, it is expected that $\nabla \cdot \boldsymbol{u}$ be zero at any location in the flow. In the (xy) observation plane, if the divergence field, restricted to the plane, is non-vanishing

$$\partial_x v_x + \partial_y v_y \neq 0,$$

then we can infer that $\partial_z v_z \neq 0$. It can be deduced that an out-of-plane flow locally exists, as the spanwise velocity gradient is different from zero. The key point here is that dynamic modes inherit the spatial properties of the velocity field, as shown in Sec. II C. Therefore, the divergence free condition, at any point of the field, should be recovered in every dynamic mode. On the contrary, a divergence free violation in any dynamic mode means that the velocity field itself is not divergence free. It is worth noticing that dynamic modes are average structures of phenomena occurring in the flow, at a given frequency. Therefore, if the divergence free condition is violated in a dynamic mode, it means that an out-of-plane phenomenon is statistically occurring in the velocity field itself. A technical point must be solved when dealing with experimental data. Because of noise, the divergence field is almost nowhere vanishing. Consequently, the inherent noise level must be

This article is copyrighted as indicated in the article. Reuse of AIP content is subject to the terms at: http://scitation.aip.org/termsconditions. Downloaded to IP: 82.230.43.64 On: Thu, 21 Aug 2014 14:08:28

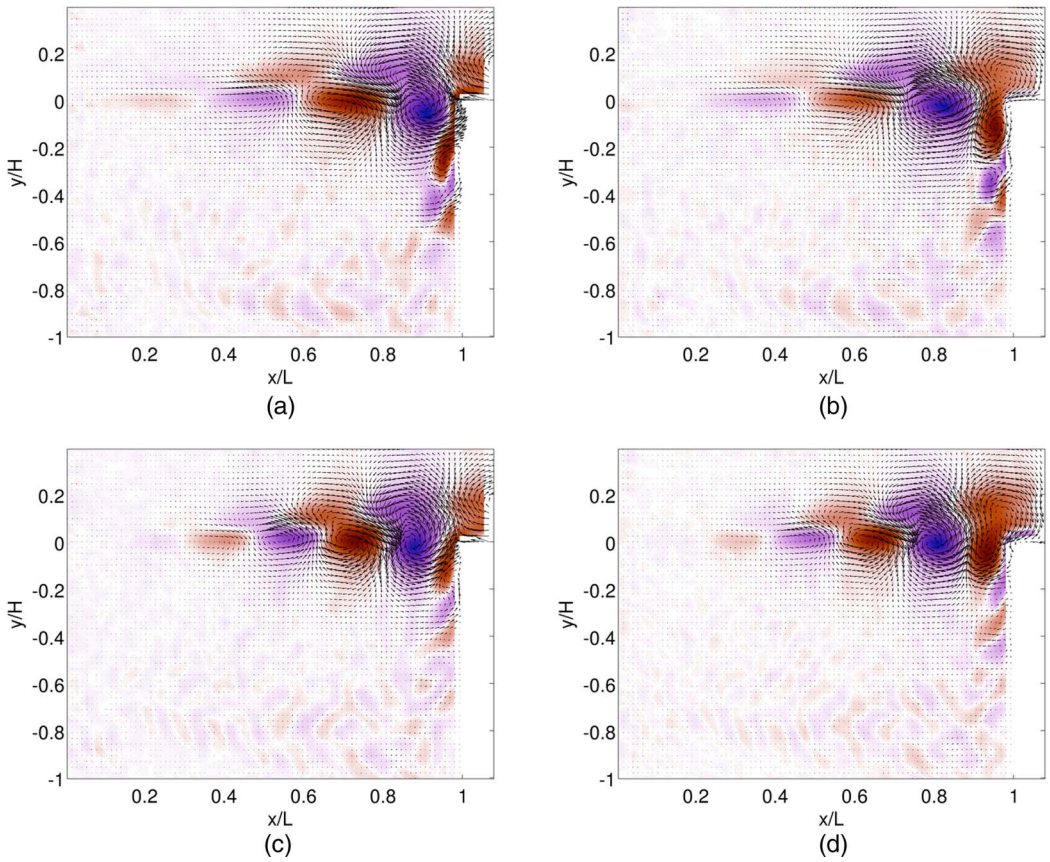

FIG. 11. DMD modes $\mathbf{\Phi}_k$ corresponding to structures in the shear layer. The color background is the vorticity field. The first line is associated with a Strouhal number $St = 1.02$, the second with $St = 1.38$. (a), (c) ((b), (d)) correspond to the real (imaginary) part of the mode.

quantified. To this end, we consider an area, $\mathcal{D}_{BL}$, where the flow is known to be planar in the (xy) plane, namely, the incoming flow, out of the boundary layer. The mean value of the divergence field in this area, $\langle \nabla \cdot \boldsymbol{v} \rangle_{BL} = \zeta_0$, will provide the reference value for vanishing divergence field, where $\langle \cdot \rangle_{BL}$ denotes the spatial average over the domain $\mathcal{D}_{BL}$. Any area in the field where the divergence value is significantly larger than this reference level will be considered as non-zero.

We first consider the dynamic modes associated with the shear-layer oscillations (Figure 11). The main result is that the shear layer modes exhibit strong non-vanishing divergence levels in the shear-layer. When we compare Figures 11(a) and 14(a), it is striking to note that the divergence field is strong where the vorticity field is strong too. The divergence field is typically one order of magnitude larger than the noise level. Therefore, the divergence field is non-zero where the flow field is coherent. This indicates that the coherent Kelvin-Helmholtz structures in the shear layer are intrinsically structured in the spanwise direction. Instead, the velocity divergence inside the cavity is not much larger than the noise level, the signal over noise ratio being slightly larger than 1. The

TABLE I. Frequency and wavelength comparison between POD analysis and DMD analysis.

	Strouhal number	λ/L
POD dominant mode	1.02 and 1.38	0.43
DMD mode $\mathbf{\Phi}_1$	1.02	0.49
DMD mode $\mathbf{\Phi}_2$	1.38	0.38

This article is copyrighted as indicated in the article. Reuse of AIP content is subject to the terms at: http://scitation.aip.org/termsconditions. Downloaded to IP: 82.230.43.64 On: Thu, 21 Aug 2014 14:08:28

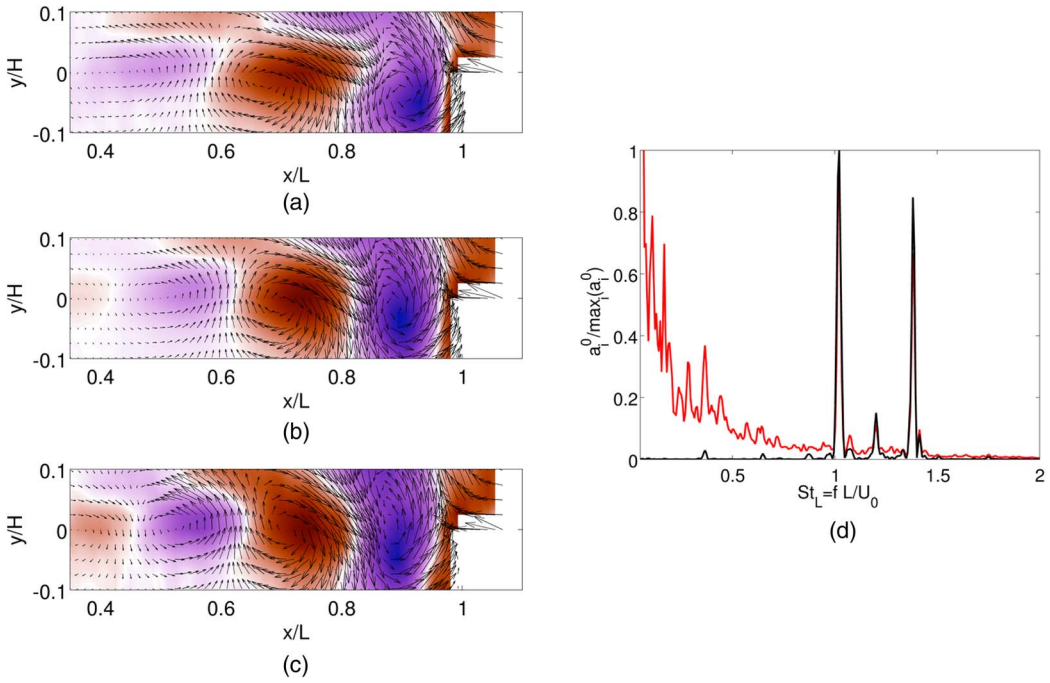

FIG. 12. Comparison of structures between shear layer modes. (a) DMD mode at $St_L = 1.02$. (c) DMD mode at $St_L = 1.38$. (b) Most energetic POD mode. The color background is the vorticity field. The Fourier (black) spectrum of the POD mode is compared with the Fourier (red) spectrum of the velocity dataset in figure (d).

velocity divergence mean levels in the different areas of the shear-layer modes are summarize in Table II.

Early spanwise modulations of the shear-layer waves were reported in experimental studies in open cavity flows, in the incompressible limit. Neary and Stephanoff[33] reported regimes with two frequencies in power spectra, the second of which they associated with spanwise modulations of the shear-layer. More recently, numerical and experimental studies on open cavity flows, both in the compressible and incompressible regimes, have considered the inner-flow complex organisation.[29,32,34] It has been reported the formation of alleys of Taylor-Görtler-like structures, as a result of centrifugal instabilities.[29,31] The characteristic scale of the patterns, in the spanwise direction, is typically of the order of H or $H/2$, depending on the selected branch of modes. Inner-flow structures can either be steady patterns or traveling-waves, depending on the control parameters. Associated Strouhal numbers based on H are typically in the range 0–0.05. The shear-layer vortices caught by dynamic modes $\mathbf{\Phi}_1$ and $\mathbf{\Phi}_2$ appear to be non-uniform in the spanwise direction. Yet, since we are only dealing with two-dimensional velocity fields, it is not possible to say whether the modulation is periodic in the

TABLE II. Measurements of the velocity divergence in some of the characteristic dynamic modes ($\mathbf{\Phi}_i, i = 0, \ldots, 5$): amplitude of the divergence level (rescaled with respect to the divergence noise reference level, ζ_0) in the shear layer S_{SL}, in the inner-flow S_{IN}, and the ratio between intensity of the velocity divergence level in the shear layer area over the velocity divergence level in the inner-flow.

Dynamic mode	St_L	S_{SL}/ζ_0	S_{IN}/ζ_0	S_{SL}/S_{IN}
$\mathbf{\Phi}_5$	0.028	3.4	5.7	0.6
$\mathbf{\Phi}_3$	0.097	3.3	4.2	0.8
$\mathbf{\Phi}_4$	0.33	3.5	3.6	1.0
$\mathbf{\Phi}_1$	1.02	8.1	1.9	4.3
$\mathbf{\Phi}_2$	1.38	11.9	1.7	7.1
$\mathbf{\Phi}_0$	0	4.5	4.5	1.0

This article is copyrighted as indicated in the article. Reuse of AIP content is subject to the terms at: http://scitation.aip.org/termsconditions. Downloaded to IP: 82.230.43.64 On: Thu, 21 Aug 2014 14:08:28

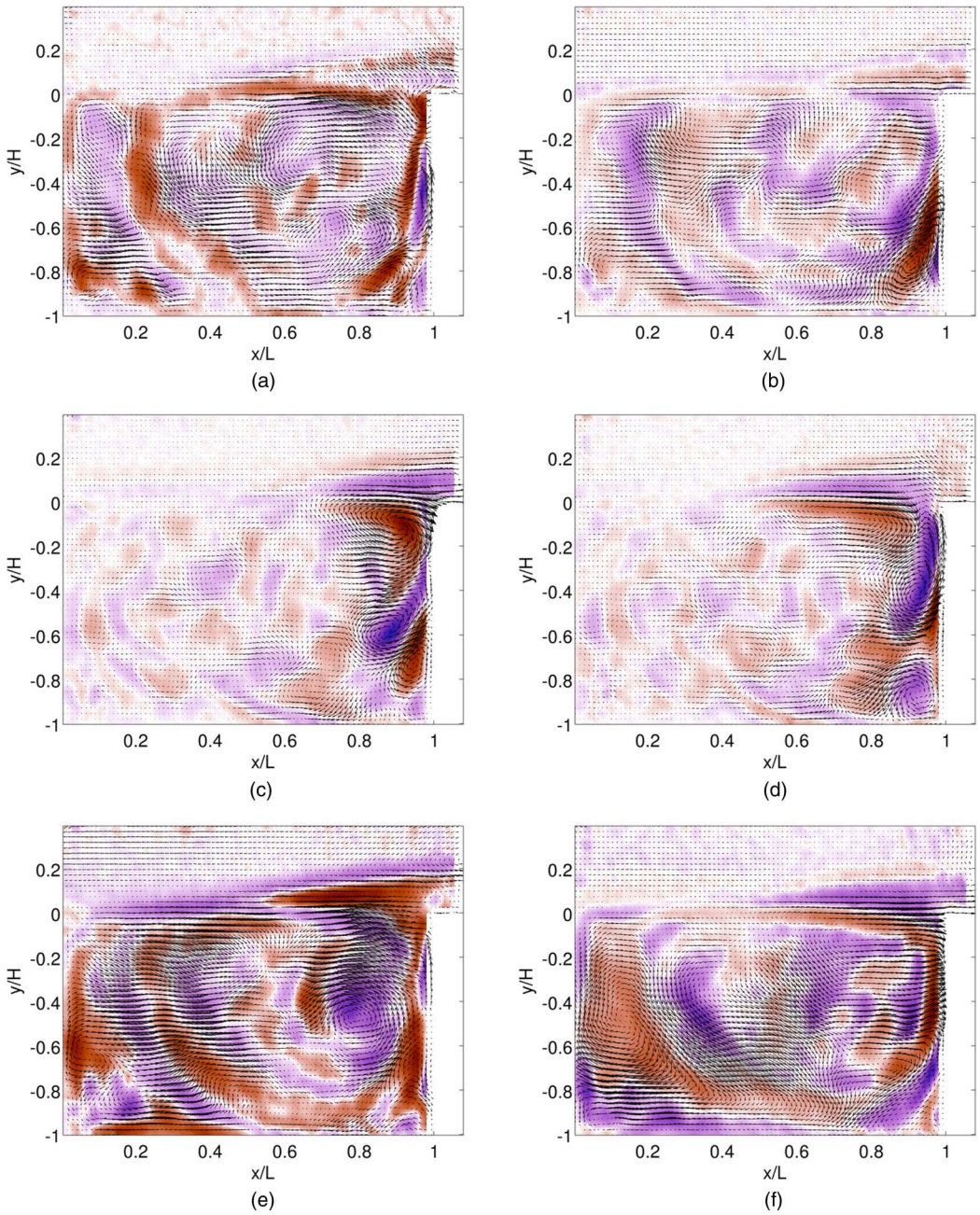

FIG. 13. DMD modes $\mathbf{\Phi}_k$ associated with low Strouhal numbers. The color background is the vorticity field. The first line corresponds to Strouhal number $St = 0.097$, the second line to $St = 0.33$, and the third line to $St = 0.028$. (a), (c), (e) ((b), (d), (f)) correspond to the real (imaginary) part of the mode.

spanwise direction or only local. Basley[29] showed how the inner-flow dynamics could couple to the shear-layer oscillations. Therefore, the non-vanishing flow divergence, in the shear-layer dynamic modes, might reveal some coupling between the shear-layer and the inner-flow dynamics.

The divergence field of the three main low Strouhal number dynamic modes is shown in Figure 15. What we learn is that the velocity out-of-plane component gradients are everywhere different from zero, inside the cavity, even though no clear structure is drawn, except in Figure 15(c). Therefore, dynamic modes at low Strouhal numbers are closely associated with spanwise flows, inside the cavity.

This article is copyrighted as indicated in the article. Reuse of AIP content is subject to the terms at: http://scitation.aip.org/termsconditions. Downloaded to IP: 82.230.43.64 On: Thu, 21 Aug 2014 14:08:28

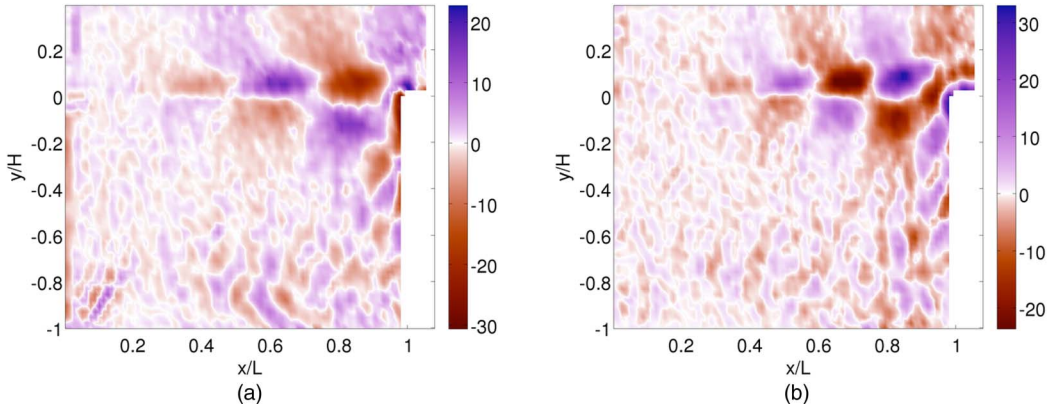

FIG. 14. Divergence field of the dynamic modes associated with shear-layer oscillations renormalized with respect to ζ_0. (a) $St = 1.02$. (b) $St = 1.38$.

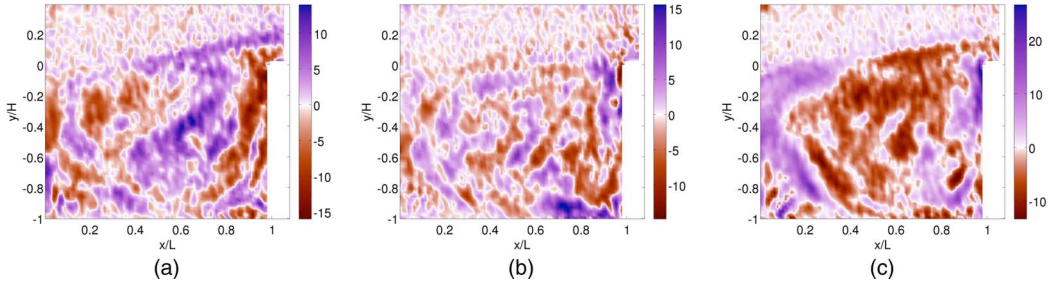

FIG. 15. Divergence field of dynamic modes associated with low Strouhal numbers renormalized with respect to ζ_0. (a) $St = 0.097$. (b) $St = 0.33$. (c) $St = 0.028$.

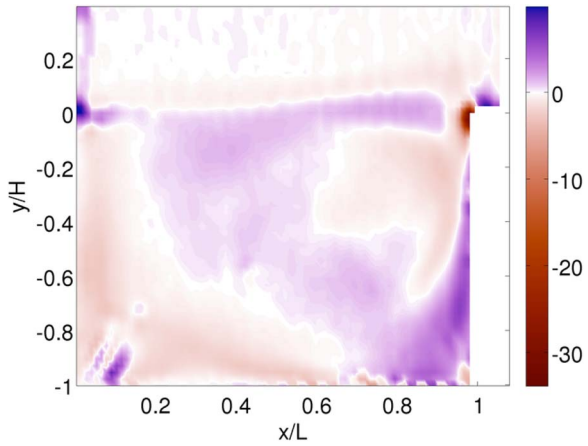

FIG. 16. Divergence of the mean flow field.

The mean flow field is shown in Figure 16, where permanent out-of-plane flows are clearly present. In particular, two opposite spanwise flow gradients are observed in the shear layer, and gradients are also strong at the cavity walls, where secondary (steady) flows are actually known to be present.[30]

This article is copyrighted as indicated in the article. Reuse of AIP content is subject to the terms at: http://scitation.aip.org/termsconditions. Downloaded to IP: 82.230.43.64 On: Thu, 21 Aug 2014 14:08:28

IV. CONCLUSION

In this study, we considered two salient features of open cavity flows. The first feature relies on the mode competition sometimes observed in the shear-layer self-sustained oscillations.[22,23] The second feature relies on the three-dimensional organisation of the inner and shear-layer flows.[19,32,33]

We tackled the study by identifying the coherent structures constitutive of the flow, from two-dimensional two-components PIV velocity fields, in a plane perpendicular to the cavity span.

We applied both POD and DMD modal decompositions. As expected for a flow whose kinetic energy is dominated by the mean-flow, the first spatial POD mode is close to the mean flow. The *chronos* of the next two dominant POD modes extract the frequencies of the shear-layer oscillations. Both *chronos* also reproduce the intermittency observed in time for the oscillations of the velocity field as exemplified by spectrograms of Figure 5. The associated *topos* exhibit vortices in the shear-layer, with wavelengths found to be the same for *topos* 2 and 3. However, the wavelength of the train of vortices in the shear layer, for those two dominant modes, is found to be the weighted average of the "true" wavelengths of the traveling waves eventually associated with each frequency. On the contrary, the true wavelengths can be identified thanks to dynamic mode decomposition. By construction, dynamic modes are associated with frequency channels. As a consequence, it is suitable for the study of intermittent phenomena, which involve well-defined frequencies intermittently present in time in the flow. Wavelengths and velocities can be estimated. We recover the expected velocities for Kelvin-Helmholtz waves involved in the instability of free shear layers, the impinging corner acting as a resonator for the allowed frequencies of oscillations.

We also considered the three-dimensional features of the cavity flow, on the basis of the coherent structures identified by dynamic mode decomposition. Dynamic modes form the spatial skeleton of phenomena that occur, in average, at a given frequency. In addition, we showed that dynamic modes, as soon as growth rates of modes are unitary, inherit the physical properties of the velocity field. Growth rates are unitary when the flow is permanent. Nevertheless, for numerical issues, we used dynamic modes computed with the companion matrix on the fluctuating flow field, which forces the growth rates to one. Consequently, dynamic modes inherit the divergence free property for incompressible flows. Therefore, a violation of the divergence free condition, in the 2D-2C dynamic mode associated with a given frequency, means that non vanishing out-of-plane flows are constitutive of the physical phenomenon caught by the dynamic mode. The numerical robustness of the divergence field is strengthen by the fact that both noise and small scales are mostly rejected into non-energetic modes.

Our study confirms that the velocity field is strongly three-dimensionally organised inside the cavity. It is obvious when considering the divergence field of dynamic modes associated with Strouhal numbers smaller than 0.05 (0.025 when the Strouhal number is based on the cavity depth). What is more surprising is that out-of-plane flows are also constitutive of shear-layer vortices. Such a feature was already suggested in previous studies, see Rockwell and Naudascher.[19] Neary and Stephanof[33] also reported wavy modulations of the main recirculation flow in peculiar configurations. From the present study, we can claim that shear-layer structures, in regime of mode competition, are intrinsically spanwisely organised vortices traveling downstream to the trailing edge.

ACKNOWLEDGMENTS

This work was supported by the French institute DIGITEO and the project FLUCTUS. The authors want to thank Jeremy Basley for fruitful discussions.

[1] J. Lumley, "Coherent structures in turbulence," Proc. Trans. Turbul. **1**, 215–242 (1981).
[2] L. Sirovich, "Turbulence and the dynamics of coherent structures. I-coherent structures. II-symmetries and transformations. III-dynamics and scaling," Quart. Appl. Math. **45**, 561–571 (1987).
[3] G. Berkooz, P. Holmes, and J. Lumley, "The proper orthogonal decomposition in the analysis of turbulent flows," Annu. Rev. Fluid Mech. **25**, 539–575 (1993).
[4] B. Noack and H. Eckelmann, "A low-dimensional galerkin method for the three-dimensional flow around a circular cylinder," Phys. Fluids **6**, 124–143 (1994).
[5] M. Bergmann, L. Cordier, and J. Brancher, "Optimal rotary control of the cylinder wake using proper orthogonal decomposition reduced-order model," Phys. Fluids **17**(9), 097101 (2005).

This article is copyrighted as indicated in the article. Reuse of AIP content is subject to the terms at: http://scitation.aip.org/termsconditions. Downloaded to IP: 82.230.43.64 On: Thu, 21 Aug 2014 14:08:28

[6] J. Jeong and F. Hussain, "On the identification of a vortex," J. Fluid. Mech. **285**(69), 69–94 (1995).
[7] J. Hunt, A. Wray, and P. Moin, "Eddies, streams, and convergence zones in turbulent flows," in *Proceedings of the 1988 Summer Program* (Stanford N.A.S.A. Centre for Turbulence Research, 1988).
[8] Z. Pouransari, M. Speetjens, and J. Clercx, "Formation of coherent structures by fluid inertia in three-dimensional laminar flows," J. Fluid Mech. **654**, 5–34 (2010).
[9] P. Schmid, "Dynamic mode decomposition of numerical and experimental data," J. Fluid. Mech. **656**, 5–28 (2010).
[10] C. W. Rowley, I. Mezić, S. Bagheri, P. Schlatter, and D. S. Henningson, "Spectral analysis of nonlinear flows," J. Fluid. Mech. **641**, 115–127 (2009).
[11] A. Seena and J. Sung, "Dynamic mode decomposition of turbulent cavity flows for self-sustained oscillations," Int. J. Heat Fluid Flow **32**(6), 1098–1110 (2011).
[12] P. Schmid, "Application of the dynamic mode decomposition to experimental data," Exp. Fluids **50**(4), 1123–1130 (2011).
[13] O. Semeraro, G. Bellani, and F. Lundell, "Analysis of time-resolved PIV measurements of a confined turbulent jet using POD and Koopman modes," Exp. Fluids **53**(5), 1203–1220 (2012).
[14] K. Chen, J. Tu, and C. Rowley, "Variants of dynamic mode decomposition: Boundary condition, Koopman, and Fourier analyses," J. Nonlinear Sci. **22**, 887–915 (2012).
[15] F. Guéniat, L. Pastur, and L. Mathelin, "Snapshot-based flow analysis with arbitrary sampling," Proc. IUTAM **10**, 25–99 (2014).
[16] F. Guéniat, "Identification de structures cohérentes dans des écoulements fluides et interfaces homme-machine pour l'exploration et la visualisation interactive de données scientifiques," Ph.D. thesis, University of Paris Sud, 2013.
[17] I. Mezić, "Spectral properties of dynamical systems, model reduction and decompositions," Nonlin. Dyn. **41**, 309–325 (2005).
[18] I. Mezić, "Analysis of fluid flows via spectral properties of the Koopman operator," Annu. Rev. Fluid Mech. **45**, 357–378 (2013).
[19] D. Rockwell and E. Naudascher, "Self-sustained oscillations of impinging free shear layers," Annu. Rev. Fluid Mech. **11**, 67–94 (1979).
[20] D. Rockwell and C. Knisely, "Observations of the three dimensional nature of unstable flow past a cavity," Phys. Fluids **23**, 425–431 (1980).
[21] D. Rockwell, "Oscillations of impinging shear layers," AIAA J. **21**(5), 645–664 (1983).
[22] M. Kegerise, E. Spina, S. Garg, and L. Cattafesta, "Mode-switching and nonlinear effects in compressible flow over a cavity," Phys. Fluids **16**, 678–687 (2004).
[23] L. Pastur, F. Lusseyran, T. Faure, Y. Fraigneau, R. Pethieu, and P. Debesse, "Quantifying the non-linear mode competition in the flow over an open cavity at medium Reynolds number," Exp. Fluids **44**, 597–608 (2008).
[24] P. Holmes, J. Lumley, and G. Berkooz, *Turbulence, Coherent Structures, Dynamical Systems and Symmetry* (Cambridge University Press, 1998).
[25] G. Kerschen, J. Golinval, A. Vakakis, and L. Bergman, "The method of proper orthogonal decomposition for dynamical characterization and order reduction of mechanical systems: An overview," Nonlin. Dyn. **41**(1–3), 147–169 (2005).
[26] D. Rempfer and H. Fasel, "Evolution of three-dimensional coherent structures in a flat-plate boundary layer," J. Fluid. Mech. **260**, 351–375 (1994).
[27] X. Gloerfelt, C. Bogey, and C. Bailly, "Numerical evidence of mode switching in the flow-induced oscillations by a cavity," Int. J. Aero. **2**(2), 193–217 (2003).
[28] J. Basley, L. R. Pastur, F. Lusseyran, T. M. Faure, and N. Delprat, "Experimental investigation of global structures in an incompressible cavity flow using time-resolved PIV," Exp. Fluids **50**, 905–918 (2010).
[29] J. Basley, "An experimental investigation on waves and coherent structures in a three-dimensional open cavity flow," Ph.D. thesis, University of Paris Sud, 2012.
[30] T. Faure, P. Adrianos, F. Lusseyran, and L. Pastur, "Visualizations of the flow inside an open cavity at medium range Reynolds numbers," Exp. Fluids **42**, 169–184 (2007).
[31] T. Faure, L. Pastur, F. Lusseyran, Y. Fraigneau, and D. Bisch, "Three-dimensional centrifugal instabilities development inside a parallelepipedic open cavity of various shape," Exp. Fluids **47**(3), 395–410 (2009).
[32] G. A. Brès and T. Colonius, "Three-dimensional instabilities in compressible flow over open cavities," J. Fluid Mech. **599**, 309–339 (2008).
[33] M. D. Neary and K. D. Stephanoff, "Shear-layer-driven transition in a rectangular cavity," Phys. Fluids **30**, 2936–2946 (1987).
[34] J. Basley, L. Pastur, N. Delprat, and F. Lusseyran, "Space-time aspects of a three-dimensional multi-modulated open cavity flow," Phys. Fluids **25**(6), 064105 (2013).

This article is copyrighted as indicated in the article. Reuse of AIP content is subject to the terms at: http://scitation.aip.org/termsconditions. Downloaded to IP: 82.230.43.64 On: Thu, 21 Aug 2014 14:08:28